Karst features interpretation using ground-penetrating radar: A case study from the Sierra de Atapuerca, Spain

Lucía Bermejo [a,b,*], Ana Isabel Ortega [a,c,d], Josep M. Parés [a], Isidoro Campaña [a], José María Bermúdez de Castro [a], Eudald Carbonell [e,f], Lawrence B. Conyers [g]

[a] Centro Nacional de Investigación sobre la Evolución Humana (CENIEH), Paseo Sierra de Atapuerca 3, 09002 Burgos, Spain
[b] Doctorado en Evolución Humana, Universidad de Burgos, C/ Don Juan de Austria, 1, 09001 Burgos, Spain
[c] Fundación Atapuerca, Carretera de Logroño, 44, 09198 Ibeas de Juarros, Burgos, Spain
[d] Grupo Espeleológico Edelweiss, Excma, Diputación Provincial de Burgos, C/Paseo del Espolón s/n, 09071 Burgos, Spain
[e] IPHES, Institut Català de Paleoecología Humana i Evolució Social, Unidad asociad al CSIC, C/Escorxador s/n, 43003 Tarragona, Spain
[f] Universitat Rovira i Virgili (URV), Campus Catalunya, Avinguda de Catalunya 35, 43002 Tarragona, Spain
[g] Department of Anthropology, University of Denver, 2000 E. Asbury Ave., Denver, CO 80208, USA

ARTICLE INFO

ABSTRACT

We used ground-penetrating radar (GPR) to identify a variety of karstic features in the archaeo-paleontological sites of the Sierra the Atapuerca (Burgos, Spain). The aim of this study was to discover the structure of the caves exposed in the 19th century by a railroad trench, specifically their bottom part, which remains covered under the railroad current surface. For this purpose, three GPR grids were made in the Trinchera area, next to the sites of the Sima del Elefante, the Galería Complex and the Gran Dolina. The analysis of both the radar wave signatures and the radar amplitude reflections, together with the existing data on the caves, allowed for the definition of the location and geometry of different karstic features, including air-filled caves, sediment-filled caves and bedrock structures. Two mechanical boreholes drilled next to the sites also added the information on the stratigraphy of the bottom part of the caves and helped with the interpretations of the GPR survey. We could distinguish between the intact geological features and the areas that were altered by the railroad construction and the later quarrying activity.

© 2020 Elsevier B.V. All rights reserved.

1. Introduction

Geophysical surveys have been widely applied in the study of archaeological sites for several decades (Hesse, 2002; Gaffney, 2008; Deiana et al., 2018). They have also been widely used for karst exploration, mainly for hydrogeological purposes. In this sense, electrical resistivity tomography (ERT), microgravity, seismic and electromagnetic methods such as very low frequency (VLF) and ground-penetrating radar (GPR), have been frequently employed to detect either air-filled or water-filled caves (Chalikakis et al., 2011; Revil et al., 2012). However, identifying caves filled with sediments using these geophysical techniques has been lacking (Weinstein-Evron et al., 2003; Valois et al., 2010; Martínez-Moreno et al., 2014). This is especially true for GPR, which has traditionally been believed to be ineffective in clayey sediments as these materials have been considered to attenuate the radar waves, limiting the depth of investigation (Doolittle et al., 2007; Piscitelli et al., 2007; Schrott and Sass, 2008; Kaufmann and Deceuster, 2014).

The Sierra de Atapuerca sites (Burgos, Spain) in the Trinchera area consist of ancient caves filled with sediments that were sectioned by a 19th century railroad trench (Figs. 1 and 2A). This trench exposed numerous cave entrances and other karst features that have been investigated over many decades and have provided outstanding Early and Middle Pleistocene archaeo-palaeoanthropological remains (Bermúdez de Castro et al., 1997; Carbonell et al., 2008; Ortega et al., 2014).

Identifying the development of this karstic system is crucial for understanding the formation processes of the sites and for planning future excavation strategies. For this purpose, the sites have been the target of ERT surveys, which were combined with information from boreholes and a variety of information about the location, dimension and direction of some karstic features (Ortega et al., 2010; Bermejo et al., 2017). GPR has been recently applied in the Sierra de Atapuerca to solve some problems related to the interpretation of ERT profiles with high resistivity values (Bermejo et al., 2016) and to obtain valuable three-dimensional analyses (Bermejo et al., 2018), which provided more detailed information than the ERT method. The two methods can be integrated, but the GPR was used in this study as stand-alone method to survey unexplored areas, otherwise extremely difficult for the ERT method.

* Corresponding author at: Centro Nacional de Investigación sobre la Evolución Humana (CENIEH), Paseo Sierra de Atapuerca 3, 09002 Burgos, Spain.
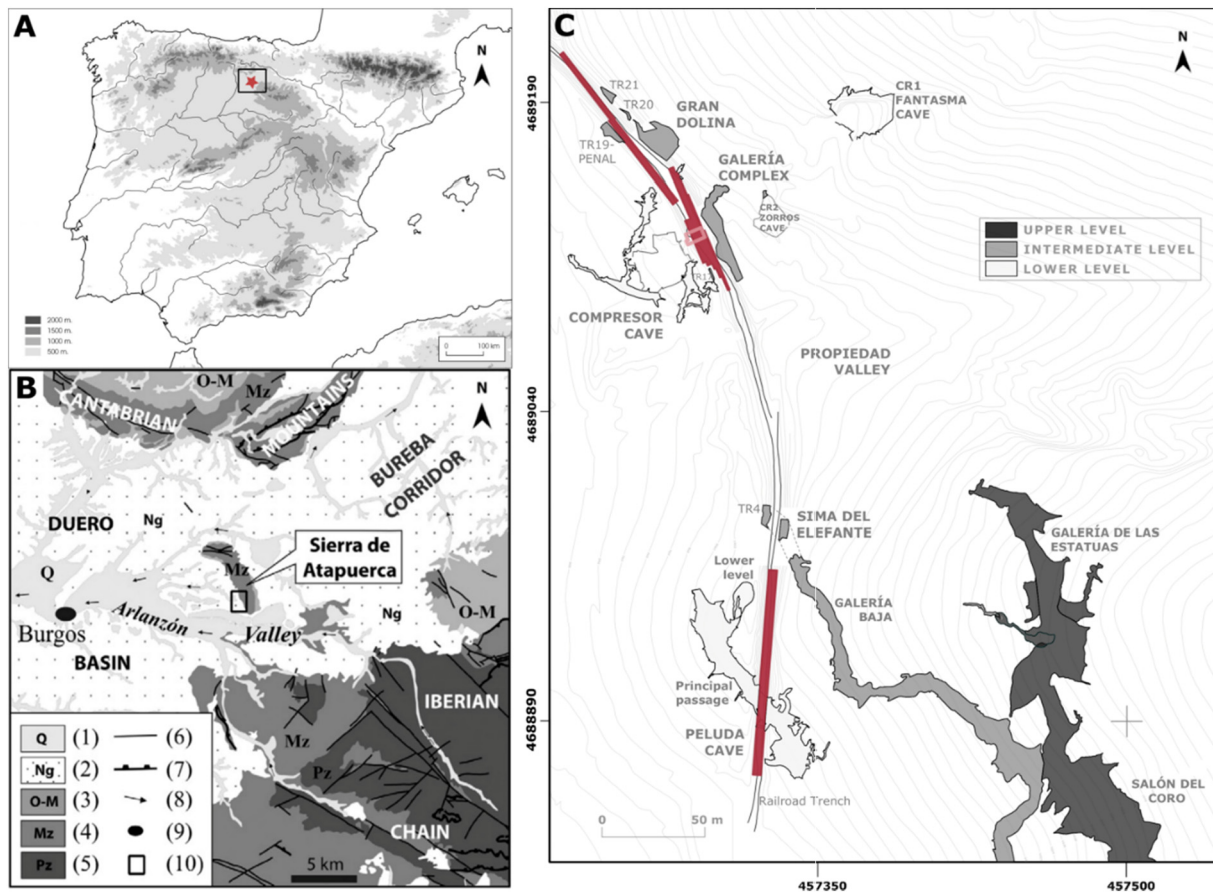E-mail address: l.bermejo.albarran@gmail.com (L. Bermejo).

Fig. 1. Location of the sites studied in this work. A) General location in Spain. B) Geological map of the Duero Basin area indicated in panel A. Legend: (1) Quaternary; (2) Neogene; (3) Oligocene-Lower Miocene; (4) Mesozoic; (5) Palaeozoic; (6) fault; (7) thrust; (8) drainage direction; (9) city; (10) area of study (modified from Benito-Calvo et al., 2008). C) Detail of the Sierra de Atapuerca multilevel cave system. The coloured polygons represent the GPR grids made over the caves. The red ones are made of longitudinal profiles and the rose polygon defines the grid of transversal profiles. (For interpretation of the references to colour in this figure legend, the reader is referred to the web version of this article.)

In the work presented here we have studied a variety of cave features that remain covered below the railroad surface with the aim of identifying their geometry and distinguishing the areas that have been altered by the railroad and the limestone quarries. Some of these areas can be currently accessed from the surface, and have therefore been studied in detail, providing models for what can be interpreted geophysically. Here we present results from three GPR grids that were collected over the caves of Peluda-Sima del Elefante, the Galería Complex and the Gran Dolina (Fig. 1). The interpretations from these GPR surveys are then compared and complemented with stratigraphic information from two boreholes and the detailed work that has been done inside the caves that are accessible.

2. Background

2.1. Geological and geomorphological settings

The Sierra de Atapuerca is a NNW-SSE gentle mountain range, composed mainly of Upper Cretaceous carbonates (Pineda and Arce, 1997), located northwest of the Iberian Chain. It is part of the Duero Basin and connected to the northeast with the Ebro Basin through the Bureba Corridor (Fig. 1B).

The Duero Basin is surficial sediments are alluvial and lacustrine deposits of Neogene and Quaternary age (Armenteros et al., 2002) that were eroded through the Plio-Pleistocene by a drainage network including the Arlanzón River and its tributaries (the Vena and the Pico Rivers), when the basin opened to the Atlantic Ocean (Benito-Calvo and

Pérez-González, 2007). This generated a stepped sequence of fluvial terraces, traditionally labelled T1 to T14, from old to young (Benito-Calvo et al., 2008), which correspond in elevation to the different passages within the Sierra de Atapuerca Cretaceous limestones (Ortega, 2009; Ortega et al., 2013). The relatively long periods of stability of the base levels produced a multilevel cave system (Ford and Williams, 1989; Anthony, 2004), which are the focus of this work.

The Sierra de Atapuerca caves are divided in three main subhorizontal levels (upper, intermediate and lower), which show a progressive migration to the west (Fig. 1C). They are strongly controlled by the structure of the host rock (Ortega et al., 2013) and encompass a total thickness of 40–70 m. The karst is split by the Propiedad Valley in two general cave systems termed the Cueva Mayor-Cueva del Silo system, which has 4.7 km of explored passages, and other caves discovered to the north of the Trinchera area by a railroad trench (from where the name *trinchera* is derived) at the end of the 19th century (Figs. 1C and 2A). The bottom part of these discovered caves is preserved below the railroad surface and therefore available for study.

Through the 20th century the Trinchera area was also used for limestone quarrying, which widened the railroad trench at some points. These operations destroyed part of some caves, but also unveiled new void spaces such as Compresor Cave (Fig. 1C) (Ortega, 2009).

2.2. The sites

In this work, we studied the bottom part of the three cave sites that are currently under archaeological excavation in the Trinchera area: the

Sima del Elefante, which is the only site of the Cueva Mayor-Cueva del Silo system sectioned by the railroad trench; the Galería Complex and the Gran Dolina (Figs. 1C and 2A). All three caves, which are filled with terrigenous sediments, are part of the intermediate level of the karst system and exhibit keyhole cross sections. The shape of these conduits results from the combination of (1) the phreatic conditions produced during a period of stability (when the adjacent rivers were neither aggrading nor degrading, and therefore the water tables were relatively stable), also expressed at the surface by the fluvial terrace T3 of the Arlazón River, and (2) the vadose entrenchments created during the subsequent base level drop that corresponds to terrace T4 (Ortega et al., 2013).

The Sima del Elefante site contains a 25 m thick cave fill divided into 16 litho-stratigraphic units (Huguet et al., 2017) (Fig. 3). These units were deposited in open cave conditions and consist of both gravity
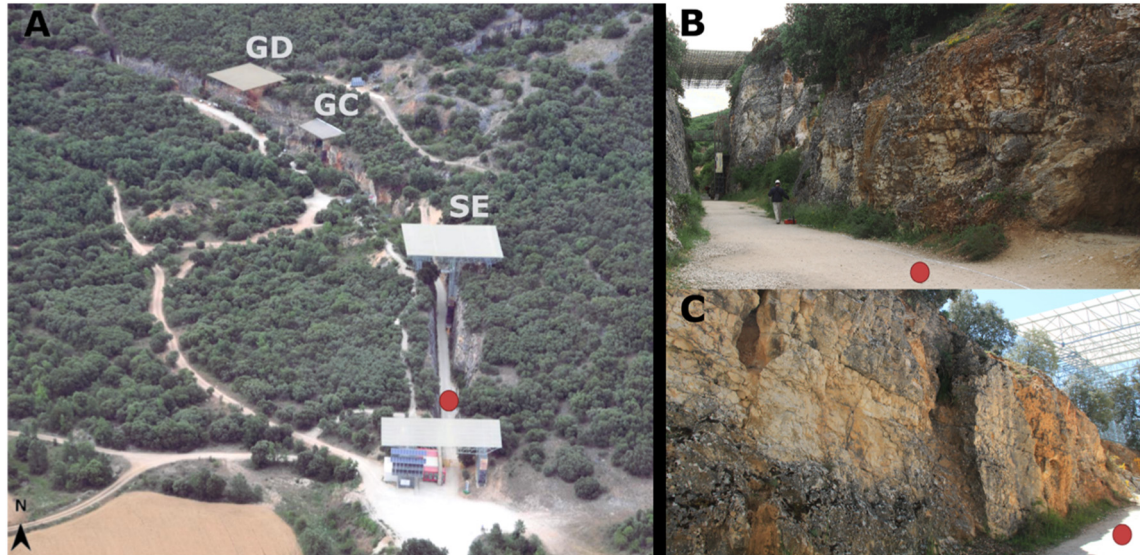

Fig. 2. A) Aerial view of the railroad trench area (photo by J. Mestre-IPHES archive) with the location of the sites studied in this work: **SE**: Sima del Elefante; **GC**: Galería Complex; **GD**: Gran Dolina. B) GPR survey over Peluda Cave (notice the cave's actual entrance on the right). Sima del Elefante site is located at the end of the picture. C) Dipping bedrock layers visible around Peluda Cave in the walls of the railroad trench. The red dot indicates the same point in all the pictures. (For interpretation of the references to colour in this figure legend, the reader is referred to the web version of this article.)
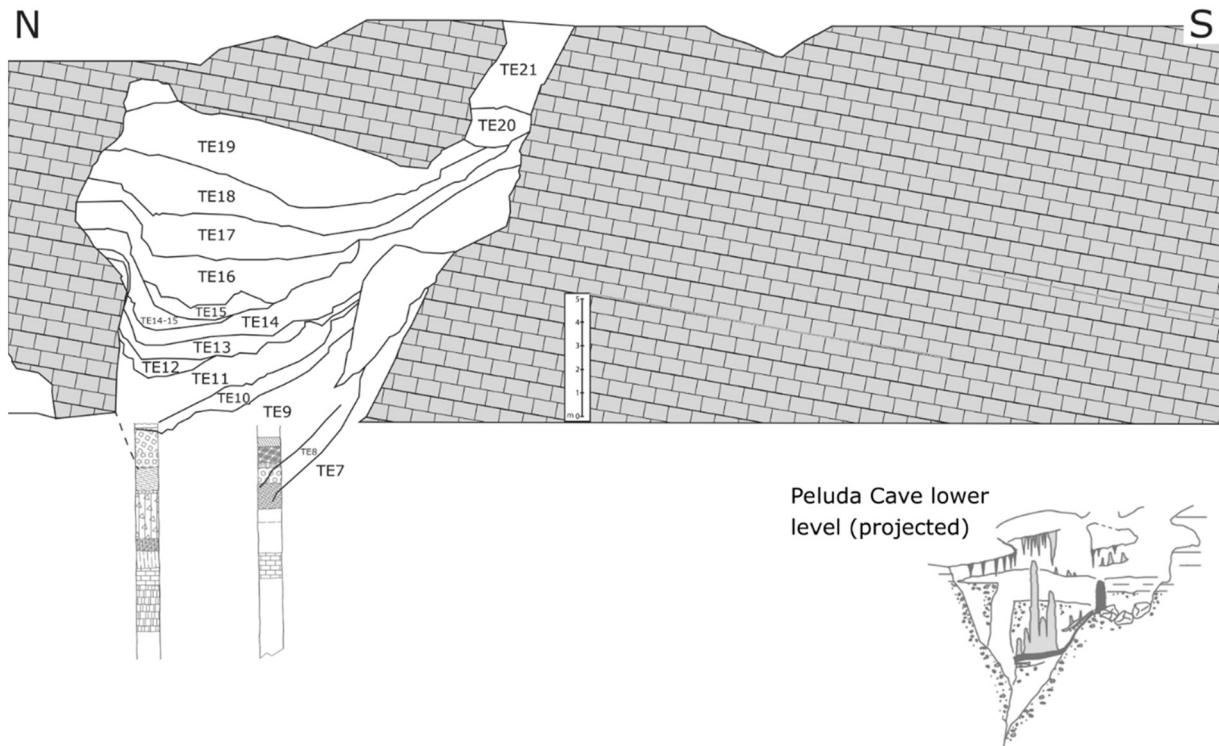

Fig. 3. Schematic stratigraphical section of the Sima del Elefante Cave (modified from Huguet et al., 2017), together with the boreholes drilled in 2001, the lower unit of which is composed of rounded quartzite pebbles (Rosas et al., 2006), and its relation with the lower level of Peluda Cave (Ortega, 2009). Notice the bedding attitude of the limestone to the south, as seen in the walls of the railroad trench (see Fig. 2C). The lower boundary of the limestone corresponds to the railroad current surface.
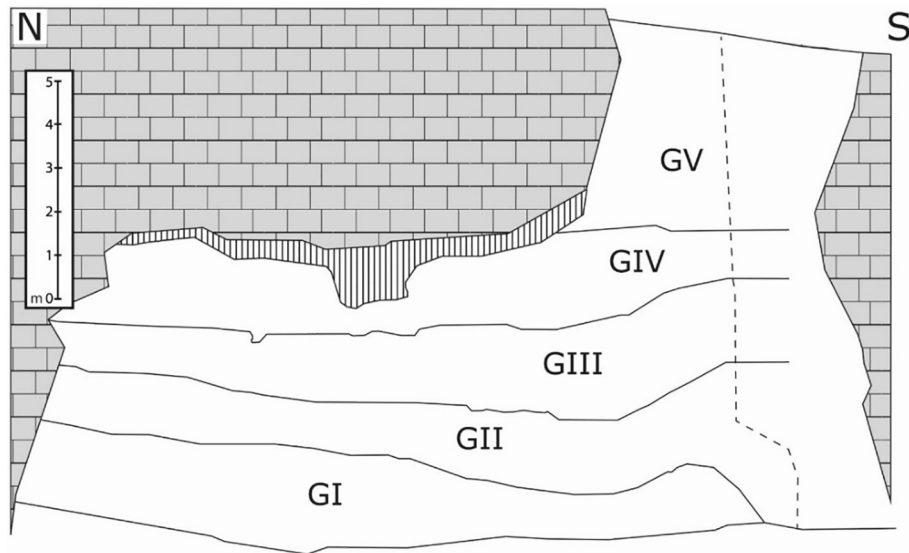
Fig. 4. Schematic stratigraphical section of the Galería Cave (modified from Ortega, 2009). The lower limit of the figure corresponds to the railroad current surface.

Fig. 5. Photographs of the eastern flank of the railroad trench: A) Galería Complex site (photo by M. A. Martín-G.E.E archive) with the identification of its principal conduits. **TZ**: Covacha de los Zarpazos; **TG**: Galería; **TN**: Northern shaft; **TC**: Central shaft; **TS**: Southern shaft. B) The railroad trench at the level of Galería Complex in 1963 (photo by J. L. Uribarrri-G.E.E archive). Notice the uneven floor of the railroad trench and the artificial mound of sediments (pointed to with an arrow) located at that time in the Propiedad Valley. C) Gran Dolina site (photo by M. A. Martín-G.E.E archive). Notice the boundary between the sediments filling the cave and the limestone host rock on the right, which was sawed during the open cut quarrying.

and water flow deposits composed of gravels and laminated clays (Rosas et al., 2006; Ortega, 2009; Ortega et al., 2014). Sediments below unit TE17 are Early Pleistocene in age (Rosas et al., 2001; Parés et al., 2006), including unit TE9, which bears the oldest European hominin fossil, dated to 1.3–1.1 Ma (Carbonell et al., 2008). These units exhibit some internal disruption, most likely because of a collapse of the lower units into a lower cave level (probably Peluda Cave) (Figs. 1C and 3) (Ortega, 2009; Ortega et al., 2018). This was a product of the adjacent river system degradation where the water table and the limestone dissolution zone were lowered during the transition from the T4 to T5 fluvial river terrace (Benito-Calvo et al., 2017).

Over time, the archaeological excavations have continued several metres below the railroad surface (Huguet et al., 2017) creating an insurmountable gap for the GPR survey. Therefore, we could only collect GPR data to the south of this cave (Figs. 2B and 3) and not directly over it.

The Galería Complex corresponds to a large and elongated chamber that received different sediment inputs. These cave entrances are, from south to north, the southern and central shafts (TS and TC) together with section TR17; the northern shaft (TN), which is the main entrance to the sub-horizontal passage of Galería (TG); and Covacha de los Zarpazos (TZ) (Figs. 4, 5A and B) (Gil et al., 1987; Ortega et al., 2013). The stratigraphic sequence of TZ, TG and TN, which reaches 13 m in thickness, is formed by five lithostratigraphic units named GI to GV, from bottom to top (Fig. 4). Unit GI is an archaeologically sterile endokarstic sedimentary deposit dated to the Early Pleistocene consisting of laminated silts and limestone breccias (Pérez-González et al., 2001). Units GII, GIII and GIV are allochthonous and composed of calcareous fluvial gravels and gravity flow deposits (Pérez-González et al., 1999). Units GII and GIII date between 500 and 250 ka (Berger et al., 2008; Falguères et al., 2013; Demuro et al., 2014) and contain a rich palaeontological and archaeological Middle Pleistocene assemblage, including two fossil hominin remains (Carbonell et al., 1999; Ollé et al., 2013), while Unit GIV is sterile.

The Gran Dolina sedimentary infill is about 25 metre thick, 19 of which are found above the railroad surface and 6 below it. It is divided into 12 lithostratigraphic units (Pérez-González et al., 2001; Campaña et al., 2016) (Figs. 5C and 6). The Early Pleistocene units (TD1 to TD7), date from about 1.2 Ma to 0.8 Ma (Moreno et al., 2015; Arnold et al., 2015; Parés et al., 2018) and are mainly composed of fluvial facies probably coeval with the deposit of the T3 and T4 fluvial terraces (Moreno et al., 2015). The Middle Pleistocene units (TD8 to TD11), date to around 0.2 Ma (Berger et al., 2008) and are dominated by gravity flow facies. The lowermost units, TD1 and TD2, are autochthonous facies deposited in close cave conditions made of clayey and sandy silts, which are archaeologically sterile. Units TD3 to TD11 are mainly allochthonous facies of mud, gravels, breccias and some layers of speleothems (Campaña et al., 2017). Units TD6 and TD10 are archaeologically exceptional. TD6 bears hominin remains of a new species, Homo antecessor, associated with primitive Mode 1 stone tools (Bermúdez de Castro et al., 1997). Unit TD10 contains two layers of abundant stone tools and fauna interpreted as having been part of a human base camp (TD10.1) and a kill site (TD10.2) (Ollé et al., 2013; Rodríguez-Hidalgo et al., 2017) respectively. The ensemble Gran Dolina-Penal, together with the nearby cave sections TR20 and TR21, were most likely part of a single cave (Ortega, 2009) (Fig. 1C).

The Penal section (Figs. 1C and 6) fill displays only a 7 metre-thick stratigraphic sequence of allochthonous facies that, according to its palaeontological remains, are correlative to the sediments of units TD4 to TD6 (Fernández-Jalvo, 1995). The lower part shows two small air-filled ascending chimneys that can be related to the lower cave level (Ortega et al., 2013). The ascending palaeocurrents inferred from the scallops visible in these chimneys suggest that this point constituted one of the main resurgences of the lower cave level (Eraso et al., 1998).

The formation of the lower cave level corresponds in time with the development of terrace T5 and T6 of the Arlanzón River (Ortega et al., 2013; Moreno et al., 2015). Terrace T7 is probably coeval with a small cave sublevel represented by the lower passages of the Silo, Compresor and Peluda caves (Ortega et al., 2014).

With regard to its sediments infills, the principal passage of the Peluda Cave shows clayey sediments with Early and Middle
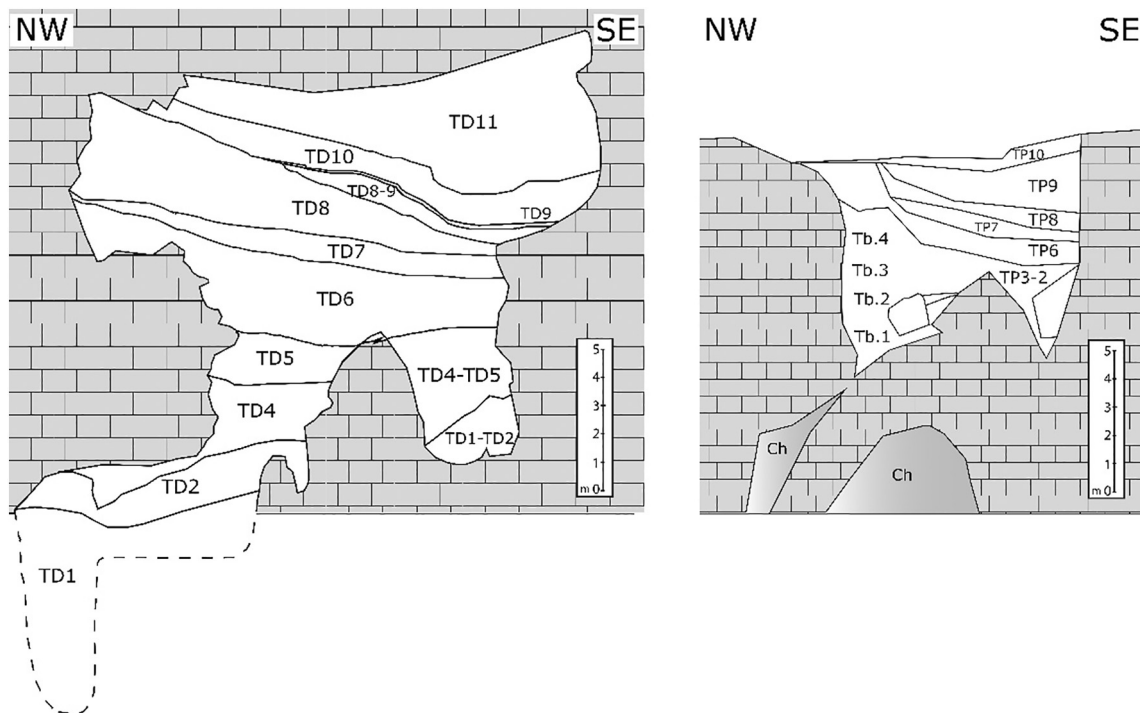

Fig. 6. Left: Schematic stratigraphical section of the Gran Dolina Cave (modified from Campaña, 2018). Right: Schematic stratigraphical section of the Penal section (modified from Fernández-Jalvo, 1995 and Ortega, 2009). Ch: air-filled ascending chimneys. The lower limit of the limestone corresponds to the railroad current surface in both images.

Pleistocene fauna and lithic remains (Ortega, 2009). The lower level of the cave contains, like the rest of the conduits of the Cueva Mayor-Cueva del Silo system, fluvial deposits that include decimetric size quartzite pebbles, sands and silts (Ortega et al., 2018) (Fig. 3). The Compresor Cave, in contrast, shows a larger void space with many chimneys (more than 10 m high). No metamorphic pebbles are found in this cave, or in the rest of the caves to the north of Trinchera (Ortega et al., 2013).

3. Materials and methods

3.1. Data acquisition and processing

Ground-penetrating radar profiles were collected with 270 MHz antennas using a GSSI SIR-300 system. Gains were manually adjusted prior to collection. The frequencies were filtered between 100 and 500 MHz and reflections were collected within a time window of 300 nanoseconds (ns).

In this work, we present the result of three GPR grids (Fig. 1C):

1. A grid of nine profiles, 100 m long each, made above the Peluda Cave and adjacent to the Sima del Elefante Cave.
2. A grid 65 × 7 m in maximum dimension consisting of fifteen profiles near the Galería Complex and the Compresor Cave. Six additional transversal profiles up to 9 m long cross this grid.
3. A grid of seven profiles with a maximum profile length of 90 m, between the sites of Gran Dolina and Penal.

All grids were georeferenced using a centimetric GPS/GNSS LEICA GS15 (Laboratory of Digital Mapping and 3D Analysis, CENIEH) and placed into a site-wide GIS mapping system.

Reflection data were processed using the GPR Viewer software (http://www.gpr-archaeology.com/software/) to remove the background noise, amplify reflections with gaining and calculate the relative dielectric permittivity (RDP) that serves as a proxy measurement for radar wave velocity (Conyers, 2013). All reflection profiles were then displayed in depth as opposed to time. In this work, we present the most representative profiles of each grid, which display the principal interpretations (Figs. 7, 11, 12B and 13).

The amplitude of reflections were also processed into depth-slices using the GPR Process software (http://www.gpr-archaeology.com/software/) that re-samples reflection amplitudes, gridding those values and interpolating between transects. The resulting reflection amplitude values were displayed in map view using Surfer 12 software (Golden Software, Golden Colorado USA). Each depth slice covered an acquisition time window of 10 ns (TWTT), which corresponds to approximately 40 cm of depth.

Amplitude maps produced in the Surfer software were exported as images and combined with the overall site karst system plan (Figs. 8 and 10) using AutoCAD (Autodesk, Inc.).

3.2. Reversed Polarity

An additional type of GPR processing used to determine void spaces was the analysis of the polarity of the radar wave reflections. This method searches for the reversed polarity (Conyers, 2012, 2013) of reflected waves that are generated when radar energy increases in velocity as it enters a void space and is then reflected back to the surface. The reflected waves generated at the cave ceiling-void space interface are different than those normally generated by bed interfaces, where velocities usually decrease as waves travel deeper in the ground. Reverse polarity waves are visible in individual wave traces as deflected in the opposite direction from the direct wave (Fig. 7).

3.3. Borehole data

To complete the information on the stratigraphy of the bottom part of the caves and to confirm the GPR profiles interpretation, two mechanical boreholes 10 cm in diameter were drilled next to the sites of the Galería Complex and the Gran Dolina (Figs. 10 and 14), with total depths of 22 and 12 m, respectively. In both cases, the boreholes encountered cave sediment infills underlain by limestone. To ensure that this limestone was the floor of the cave, the drilling continued for two more metres. The boreholes' stratigraphy is displayed in Fig. 14 and discussed in Section 4.2.3 below.

4. Results and interpretation

There are four main features that we could identify in the GPR interpretation: air-filled caves, sediment-filled caves, bedrock layers and structures of anthropic origin. To produce images of these features GPR profile analysis was performed accompanied by amplitude mapping. Each of the cave systems will be discussed with respect to their features, and how those were analysed.

4.1. Cueva Mayor-Cueva del Silo system: Peluda Cave and Sima del Elefante

4.1.1. Air-filled caves

The high amplitude reflections visible around distances 23 to 44 (Figs. 7 and 8) correspond to the 2–2.4 m high void space of the Peluda Cave found under the railroad trench. The most significant reflection in the GPR profiles was produced at the cave ceiling-void interface, where there is a contrast between the limestone bedrock and the air. This ceiling-void reflection interface is confirmed by the reversed polarity of those waves (Fig. 7). There is also a high amplitude reflection produced from the floor of the cave, which displays a "velocity pull-up", common when radar waves move in air at the speed of light within the void, and therefore the cave floor reflections are recorded in less elapsed time than surrounding bedrock layers (Conyers, 2013). For this reason, the void space appears in the GPR profile to have only a height of 1.5 m, where the actual height is 2.4 m (Figs. 7 and 9). Because of this velocity pull-up, the floors of the caves are sometimes visible as reflections that arch upward, which is the case of the one found around distances 23 to 26 (Fig. 7). On the contrary, both the reflections of the floor and the ceiling of the cave that are visible around distances 27 to 43 dip to the south. This is consistent with the observations of these features within the cave (Fig. 9).

There is an interesting area within the Peluda Cave void that has no visible radar reflections (Fig. 8). This corresponds to an area in the cave with vertical columns (Fig. 9) that do not reflect radar energy back to the surface, as the downward propagating radar waves move parallel to the columns walls and are not reflected.

The high amplitude reflections at distances 47 and 59 (Figs. 7 and 8) probably correspond to additional void spaces such as chimneys, which are unknown at the present.

4.1.2. Sediment-filled caves

A reflection between distances 18 to 20 shows a passage filled with sediments in the Peluda Cave, which displays a high amplitude ceiling reflection. However, no floor reflection (Fig. 7) is visible here, which suggests that the radar energy has been attenuated by cave fill. This sediment-filled conduit is likely an un-explored branch of the Peluda Cave (Fig. 8), whose entrance has not yet been discovered.

There are also high amplitude reflections between distances 42–45 (Figs. 7 and 8) at a depth of 1.8 m that may correspond to the entrance opened during the construction of the railroad, which was documented by the locals in the early 20th century. That entrance was a former chimney of the Peluda Cave, which was subsequently filled by the debris of the railroad trench. The radar reflections are likely generated from that fill, which is still visible in the cave (Ortega, 2009).
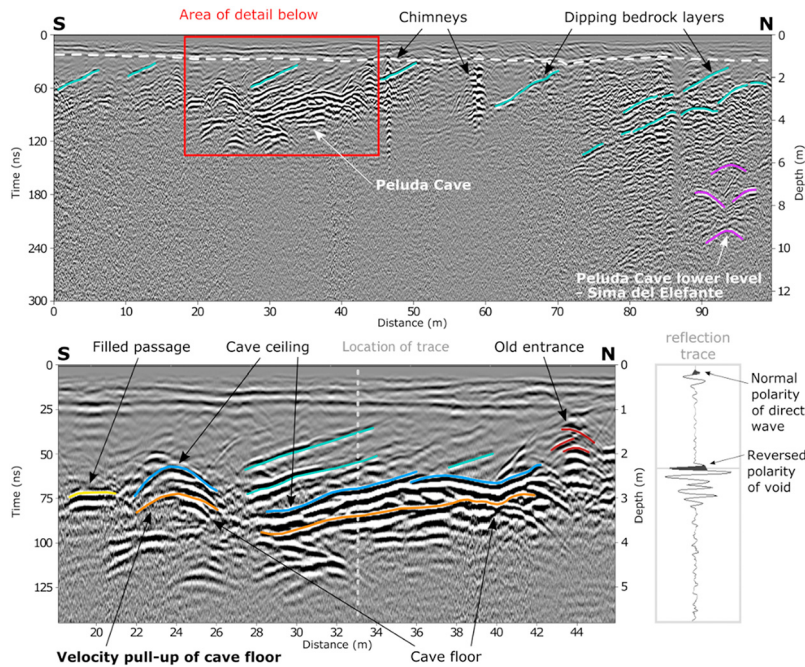
Fig. 7. Interpretation of the GPR profile 4. This profile is located in the middle of the grid collected over Peluda Cave (Figs. 1C and 8). The white dashed line marks the extent of the railroad debris fill. The cyan lines display dipping bedrock layers. (For interpretation of the references to colour in this figure legend, the reader is referred to the web version of this article.)

Reflections visible between distances 88 and 100, as deep as 6 m (Fig. 7), correspond to the lower level of the Peluda Cave (Fig. 8). Here, both the ceiling and the floor of the cave generated radar reflections, unlike other sediment-filled caves where no floor reflections are visible. This is probably because the conduit is filled with some type of sediment that allows the passage of radar waves more readily. One possibility is that this fill is composed of quartzite pebbles in a sandy-clay matrix (Fig. 3), a deposit that has also been found in the lower level of the Cueva Mayor-Cueva del Silo system (Ortega et al., 2013). These types of sediments have been noted elsewhere to be an excellent medium for radar wave penetration with little energy attenuation (Conyers, 2013).
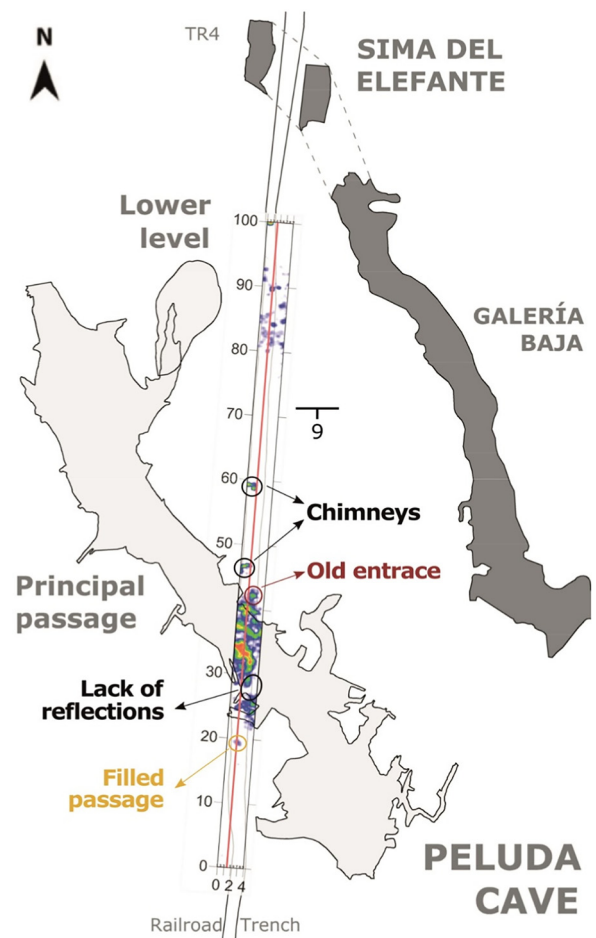
4.1.3. Bedrock layers

The dipping reflections that are visible in all GPR profiles (Fig. 7) were generated at the bed contacts in the limestone host rock. They all exhibit an apparent dip of 9° to the south, which is consistent with the bedding visible in the walls of the railroad trench (Fig. 2C). The fact that the caves preferentially developed along bedding planes is visible in the GPR profiles, where they show the same dip than the ceiling of the cave (Fig. 7), as well as within the Peluda Cave (Fig. 9).

4.1.4. Anthropic structures

The horizontal reflections visible in the top metre of all GPR profiles correspond to the anthropic fill produced during the railroad construction in the trench (Fig. 7). These layers were excavated at the Sima del Elefante (Fig. 3) showing about 1 m of debris fill, which included the wooden sleepers of the tracks and the stone ballast of the railroad. Identifying this railroad debris is important because its undisturbed presence indicates that there has not been any post railroad activity in the area.

4.2. Northern caves of Trinchera: Galería Complex and Gran Dolina

The main characteristic of the sediments that fill the caves located to the north of Trinchera is that they do not generate radar reflections. However, the location of these no reflections areas is indicative of cave sediments infills.
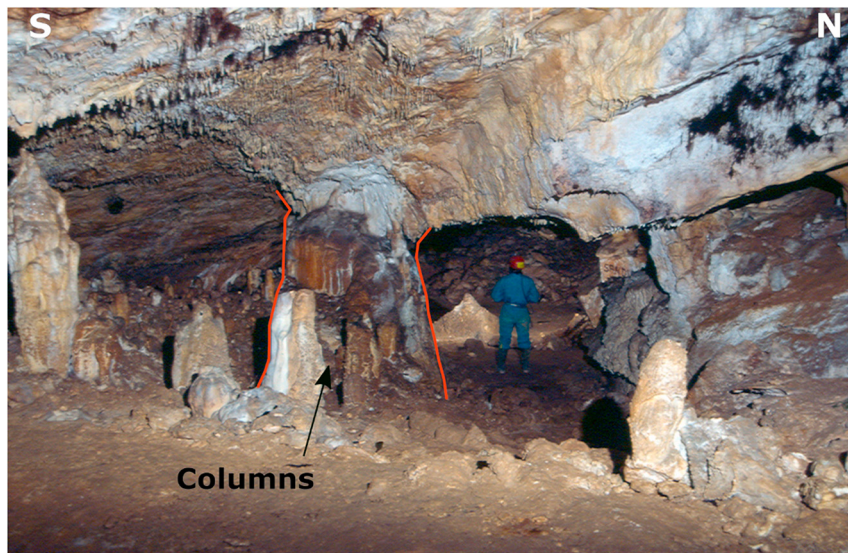

Fig. 8. Slice map (2.60–3 m deep) of the GPR grid made over Peluda Cave and its interpretation. The red line indicates the location of the GPR profile 4, shown in Fig. 7.

Fig. 9. View of Peluda Cave (photo by M. A. Martín-G.E.E archive). Notice the columns as well as the bedding of the host rock, visible on the ceiling.

4.2.1. Galería Complex

4.2.1.1. Sediment-filled caves. At the Galería Complex, the area of no-reflection visible in the first 20 m of the amplitude map corresponds to the cave sediments of the southern (TS) and the central (TC) karst shafts (Figs. 5A and 10). As there is no record of the southern wall of TS in the GPR profiles (Fig. 11), this sediment-filled conduit must continue to the south.

A wall of bedrock separates this infill area from the one of the northern shaft (TN), Galería (TG) and Zarpazos (TZ) (Figs. 5A, B, 10 and 11). To determine the depth of the cave floor, a borehole was drilled in this area (Fig. 10), which revealed 17 m of cave fill sediments overlying the bedrock. These sediments are composed of fine-grained sands and clays (see a more detailed description in Section 4.2.3), which is consistent with unit GI.

The gap where there are no high amplitude reflections around metre 60 in the amplitude map is related to an air-filled vertical chimney exposed on the eastern side of the trench (CE) (Fig. 10). According to the direction of the walls of both the chimney and the northern gallery of Compresor Cave, this infill area could be a sediment-filled passage of the same cavity (Figs. 10 and 11).

4.2.1.2. Bedrock layers. Two different groups of reflections generated by the narrow conduits developed along bedding planes of the limestone can be distinguished in the GPR profiles of the Galería Complex (Figs. 10 and 11). The reflections from the bedding planes of group A appear to be almost flat (Figs. 11 and 12B). In contrast, the bedding planes of group B (Fig. 11) show an apparent dip of 6° to the SSE, while considering all the GPR profiles the true dip is of 19° to the southwest. Therefore, these reflection profiles cross at least two different bedding attitudes of the limestone host rock, which are not visible in the walls of the trench at simple sight.

There are distinct discontinuities between the highly reflective limestone bedding planes and the cave fill sediments. Those boundaries (marked by a red line in Fig. 11) are the shape of the cave walls prior to sediment filling and mimic the typical sinuous outlines of the cave walls known in this area.

4.2.1.3. Anthropic structures. The historical quarrying activity was especially intense on the west flank of the trench, towards the Compresor Cave, where there was an underground mine (Fig. 10). The ramp used to extract the blocks from this mine is visible in some of the transversal GPR profiles (Fig. 12B). Therefore, we assume that everything on top of
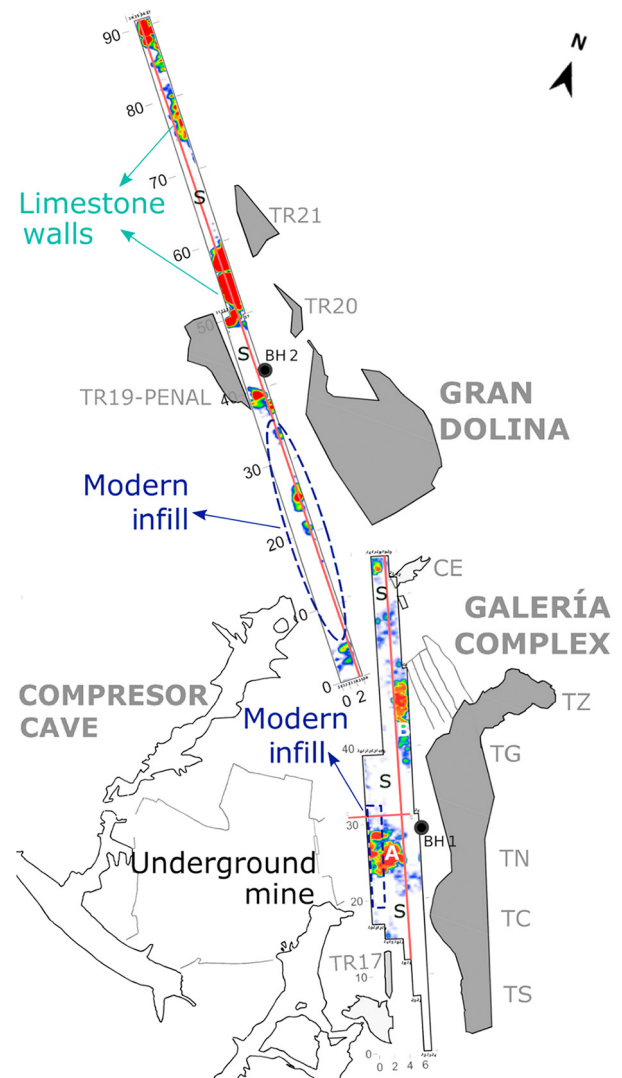

Fig. 10. Slice maps of the GPR grids made over Galería Complex and Gran Dolina corresponding to a depth of 3.20–3.60 m. The letter S indicates the areas interpreted as karstic sediment fills. The red lines indicate the location of the GPR profiles shown in Figs. 11, 12B and 13. (For interpretation of the references to colour in this figure legend, the reader is referred to the web version of this article.)
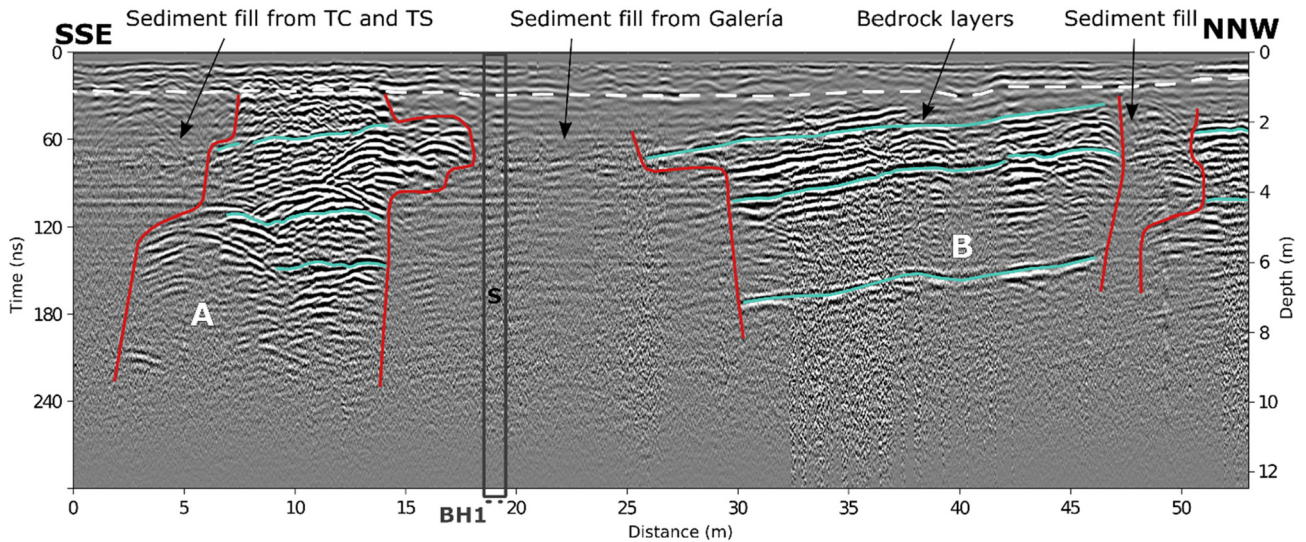
Fig. 11. Interpretation of the GPR profile 19. This profile is located in the middle of the grid made in Galería Complex (Figs. 1C and 10). The white dashed line marks the extent of the railroad debris fill. Notice that the metre 0 of this profile is not at the same point than the one of Fig. 10. The letter S indicates cave fill sediments in the borehole BH1, as shown in Fig. 14.
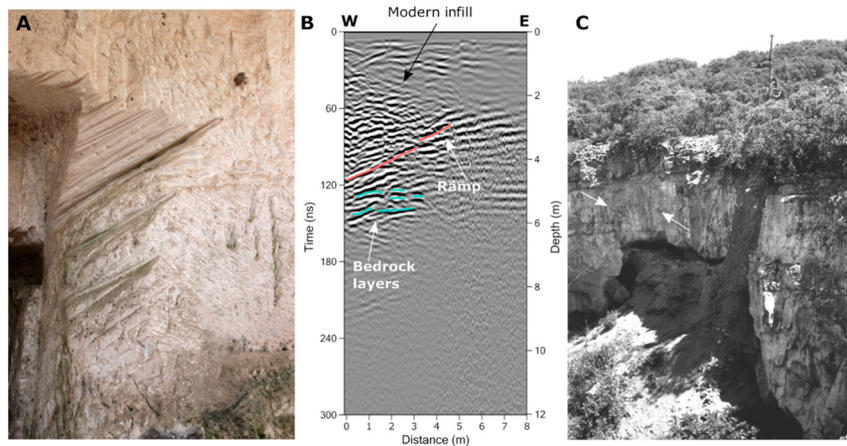

Fig. 12. A) Grooves left by the pulling wire in the wall of the Compresor Cave mine (photo by L. Bermejo). B) Interpretations of the GPR profile 27. This profile is located in the middle of the transversal smaller grid made in Galería Complex (Figs. 1C and 10). C) Galería Complex site in 1964 (photo from the F. Jordá archive). Notice the pulley on top of the trench and the wires (pointed to with arrows) used to pull the blocks from the underground mine up to the railroad trench floor.

it (up to 4 m) corresponds to a recent debris fill and the reflections east and under the ramp, to original geological features. Examining both the longitudinal and transversal profiles, we have estimated the extent of this altered area, which is shown in Fig. 10.

4.2.2. Gran Dolina

4.2.2.1. Sediment-filled caves. In the profiles collected at the Gran Dolina, an area of no radar wave reflection about distance 45 corresponds to the sediment fill of this cave (Figs. 5C, 6, 10 and 13). The borehole drilled in this area (Fig. 10) revealed that this sediment fill is composed of 10 m of silts and clays (see a more detailed description in Section 4.2.3), as seen in unit TD1 (Campaña, 2018; Parés et al., 2018). This stratigraphy confirms what can be seen in all GPR profiles where cave infill produces no reflections and radar energy is attenuated. In these areas the cave floor is invisible as all radar waves were attenuated before reaching that depth (Fig. 13).

In contrast, the cave floor of TR21 is visible in the GPR reflection profiles at a depth of 6 m, indicating that the sediment fill of this cave is sedimentologically different from that in Gran Dolina. While no sediment analysis was done, it is possible that these sediments contain less

attenuating clay than other cave fills. Therefore, these sediments could be similar to the cemented sands found at the railroad surface level in the cavity TR21 (Ortega, 2009).

4.2.2.2. Bedrock layers. The high amplitude reflections of these profiles correspond to the limestone bedding planes, the edges of which show sinuous outlines consistent with cave walls (Fig. 13).

4.2.2.3. Anthropic structures. From distances 6 to 35 there is a 2 m deep no-reflection area (Figs. 10 and 13) that corresponds to the irregular terrain left by the extensive limestone open cut quarry (Fig. 5C). This area was filled with the sediments from an artificial mound located until the 1990s in the Propiedad Valley (Fig. 5B), which could explain the lack of reflections. This altered area is defined by the lack of railroad debris fillings, which are distinguishable again at about distance 37 (Fig. 13), indicating the extent of post railroad activity.

4.2.3. Boreholes description

Both boreholes 1 (BH1) and 2 (BH2) encountered about 1 m of recently deposited sediments at the top, associated mainly with the railroad debris fill (Fig. 14). Below that layer, in the Galería Complex borehole
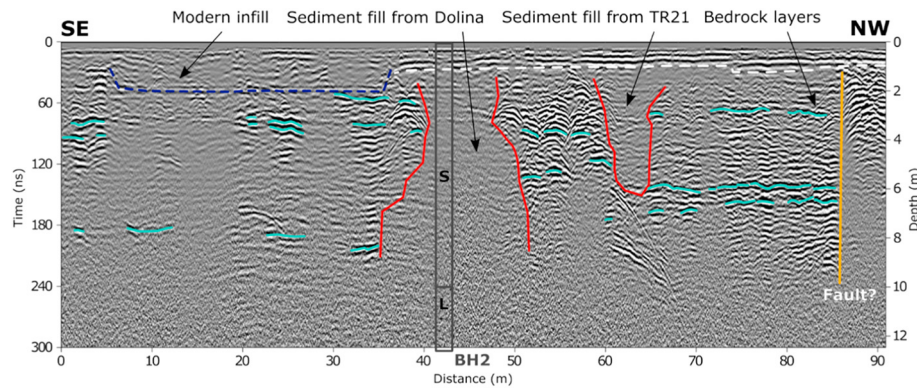
Fig. 13. Interpretations of the GPR profile 35. This profile in located in the middle of the grid made in Gran Dolina (Figs. 1C and 10). The white dashed line marks the extent of the railroad debris fill. The letter S indicates cave fill sediments in the borehole BH2 and the letter L the limestone floor of the Gran Dolina cave, as shown in Fig. 14.
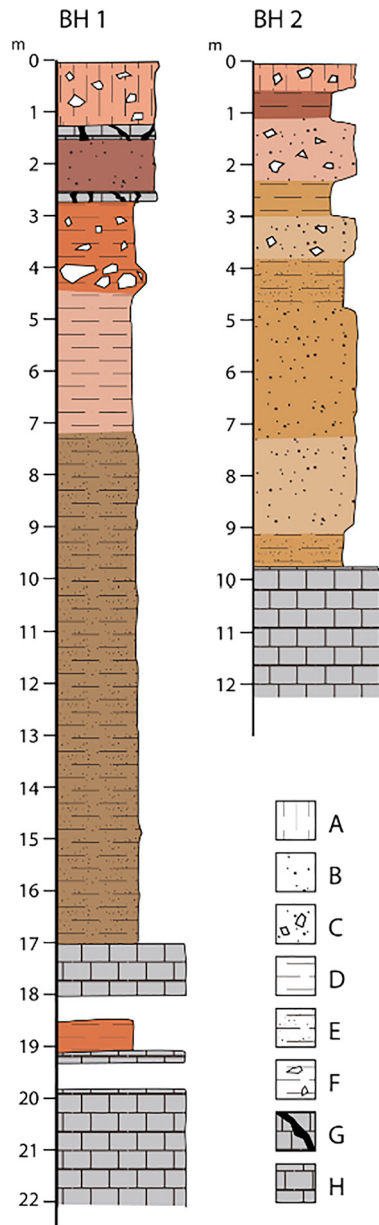

Fig. 14. Lithological description of borehole BH1 (Galería Complex) and borehole BH2 (Gran Dolina). Legend: A: railroad debris fill; B: fine sands; C: fine sands with limestone clast fragments; D: fine clays; E: clayed sands; F: fine clays with limestone clast fragments; G: limestone fragments; H: limestone host rock.

(BH1) there is a layer of fine sands, which is found between two fragments of limestone, followed by more than 1 m of fine clays with centimetric limestone clast fragments, more than 2 m of fine clays, and 10 m of clayed sands. At the bottom of this borehole there are 2 m of limestone (possibly a block), underlain by a 30 centimetre-deep void space, a 50 centimetre-thick layer of fine clays, another limestone block 20 centimetre-thick, and another 50 centimetre-deep void, before reaching the limestone host rock (Fig. 14). These sediments are similar to the autochthonous facies visible in unit GI, described as a succession of laminated and massive sand and clay layers (Pérez-González et al., 2001).

The Gran Dolina borehole (BH2) shows an alternation of 4 layers of fine clays and fine sands with centimetric limestone clast fragments, thinner than 1 m each. Then, there is a layer of about 1 m of clayed sands, 4 m of fine sands, and a 80 centimetre-thick layer of clayed sands (Fig. 14). This matches the 6.5 m deep stratigraphy of the sediments of unit TD1 found under the railroad surface, which are described by Campaña (2018) as a succession of millimetric layered sandy silt and clay facies with a thickness that ranges between 1.5 m and 20 cm.

Even though the limitations of the mechanical drilling, the available information on the sediment types and depths corresponds well with our GPR reflection profiles and geomorphological interpretations.

5. Discussion

5.1. Karstic features

The GPR surveys conducted at the Trinchera caves allowed us to identify a variety of karst features, such as air-filled caves, sediment-filled caves and bedrock layers, depending on the characteristics, orientation and reflectivity of the recorded radar reflections. The depth-slices (Figs. 8 and 10) show that the boundaries between all these features are well defined by GPR, as the amplitude reflections match accurately the cave maps.

However, not all these features visible in GPR profiles are located at accurate depths. One example is the case of the Peluda Cave, where the change in radar wave velocity when entering the void space created a velocity "pull up" (Fig. 7) of the cave floor. As shown by Bermejo et al. (2018), the difference between the real depth of the floor and its location on the GPR profile is greater in the tallest part of the cave. In those areas radar waves travelled a greater distance in air at the speed of light, creating a larger velocity pull-up.

Another example are the sediments that fill the caves, which in most cases are composed of electrically conductive clays (as shown by ERT) (Bermejo et al., 2017) and have attenuated the radar waves so that the cave floors below these sediment infills are invisible with GPR, usually below about 5–6 m depth. This is particularly the case in the Gran Dolina, where the radar wave did not reach the floor of the cave (Fig. 13), which is found within the survey time-window according to the borehole made in this area (Fig. 14). It could be argued that the

invisibility of these cave-fill sediments may also be a product of the thin layers described in Campaña (2018), as 270 MHz antennas cannot resolve bedding thinner than about 30 cm (Conyers, 2013). However, the sediments recovered from the borehole BH2 (Fig. 14) showed that there are major sedimentary changes that could have generated reflections if the radar wave had not been attenuated.

The sediment fill of TR21 is the only cave to the north of the Trinchera that recorded a reflection from the floor of the cave. This suggests that these sediments contain less clay and are therefore less electrically conductive than the rest of the cave fills, indicating that they could be more like the cemented sands visible at the railroad surface level in TR21 (Ortega, 2009). In addition to the identification of different sediment types, the fact that both caves have the same orientation (Fig. 15) indicates that the Gran Dolina Cave and the TR21 cavity are not connected under the railroad surface, even though their exposed morphologies suggest that they correspond to different sections of the same cavity (Ortega, 2009). Perhaps they were connected only during their phreatic formation, before changing into vadose conditions.

Fig. 15. Map of the underground unaltered karstic features interpreted in this study according to the GPR profiles and slice maps. The different karstic infills are represented in red (gradients mean an unknown limit) and the limestone host rock bedding planes are indicated for each area. The previously known cave fillings are represented in grey. (For interpretation of the references to colour in this figure legend, the reader is referred to the web version of this article.)

Another type of radar reflections recorded from cave sediments without such an attenuation is found at the Peluda Cave (Fig. 7). Here there was good radar energy penetration, with reflections produced at depths between 6 and 10 m. These reflections may correspond to the ceiling and the floor of the lower passage of the Peluda Cave, which shows fluvial deposits composed of quartzite pebbles in a sandy matrix at this depth (Ortega, 2009) (Fig. 3). The same deposits were found 6 m below the railroad surface in the boreholes made in 2001 in the Sima del Elefante (Rosas et al., 2006) (Fig. 3). This supports the hypothesis that the Peluda Cave and the Sima del Elefante Cave are connected at this depth (Rosas et al., 2001 and 2006; Ortega, 2009; Huguet et al., 2017; Ortega et al., 2018), as the passage identified in the GPR profiles is found halfway between both caves. According to this data, the caves could be linked by a 4 m tall passage, probably filled by this quartzite pebble fluvial terrace, which would also not have attenuated the radar waves as much as other cave sediment infills. Future GPR surveys might be able to identify in detail such a connection, which has not yet been discovered by cave explorers.

The GPR survey has also provided significant information on the three-dimensional structure of the bedrock layers. We have identified 4 dissimilar bedrock areas according to bedding attitude: the area of Peluda, whose horizons dip 9° to the south (Figs. 2C and 7) and which is the only one visible at simple sight in the walls of the trench; the area related to the wall that separates TC and TN, which shows subhorizontal bedding (Figs. 11 and 15); the one of Galería, where beds dip 19° to the southwest according to our calculations (see Section 4.2.1) (Figs. 11 and 15); and the one in Gran Dolina and TR21, which shows also subhorizontal bedding (Figs. 13 and 15). At a large scale, however, we could consider that there are actually two areas, as far as bedding attitude, south and north of the Propiedad Valley. Bedding to the southwest in Galería could be related to an E-W fracture, which is a common fault direction in the Sierra de Atapuerca and has determined to large extent the course of the Propiedad and Arlanzón Valleys (Benito-Calvo and Pérez-González, 2015).

Finally, there is important geomorphological information concerning the caves' formation processes that can be determined from our results. GPR profiles show that there is a deep incision at the bottom of all the caves of the Trinchera area, as deep as 17 m in some cases (Fig. 14). Moreover, all visible cave infills found along the railroad trench extent well below the railroad surface (Fig. 15), even though sections of the western flank do not suggest this (Fig. 6). Recent excavations of the Sima del Elefante Cave have already shown this to be the case for this site (Huguet et al., 2017).

Our observations highlight the intense vadose entrenchment incision at the Trinchera area, which is possibly related to time interval between fluvial terraces T3-T4 (Ortega et al., 2013; Benito-Calvo et al., 2017), and suggest that this area continued to be active during the formation of the lower level of the karst. In some cases, like in Galería Complex, the GPR survey has identified the lateral limits of the caves, but their continuation to the west of the trench is unknown for others (Fig. 15).

5.2. Anthropic structures

Three main anthropic activities have left their imprint in the Trinchera area: the construction of the railroad trench, the limestone quarries and recent infills.

Different archaeological works have recovered remains of the railroad ballast, sleepers and nails (notably during the expansion of the excavation of the Sima del Elefante) under the railroad current surface, which correspond to the horizontal reflections visible from the surface to 1–1.5 m deep in the GPR profiles (Figs. 7, 11 and 13). The preservation of this debris fill is a good indicator that there was no further anthropic activity in these areas and that the stratigraphy recorded below the trace of the railroad has not been altered.

Among the quarry activities that took place in the Trinchera area from the 1950s to the 1970s, the underground mine developed in the
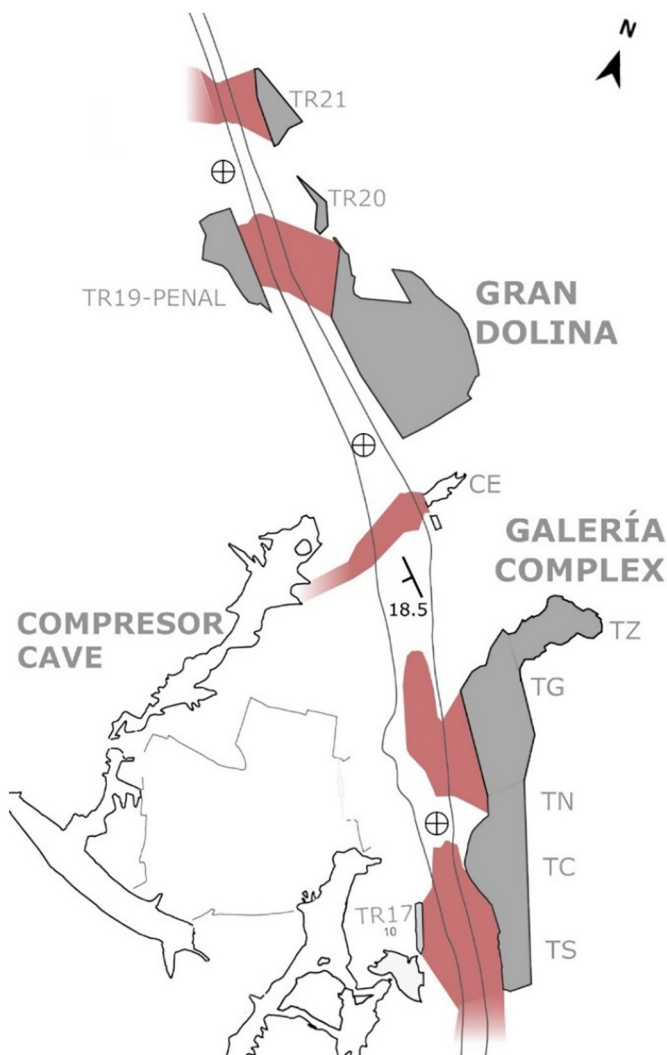
Compresor Cave was the most intense exploitation. The blocks of this mine were pulled, through a ramp, to the trench floor by a pair of wires (Fig. 12C). These have left grooves at an angle of 30° on the walls of the mine (Fig. 12A), which suggests that the reflections with a similar inclination found in some of the transversal profiles (Figs. 1C, 10 and 12B) correspond to the ramp used for extracting the blocks. This altered area is limited to the western flank of the trench and to a section that matches the walls of the mine (Fig. 10), meaning that the rest of the karstic features should be preserved unaltered under the railroad debris fill, which can be identified in the rest of the profiles (e.g. Fig. 11). As for the open-air quarries, the extractions mostly took place over the walls of the trench, principally in the area between the Galería and the Gran Dolina, where a sawed wall is still visible today (Fig. 5C). In the GPR profiles the trace of this activity is recorded to the south of the Gran Dolina, according to the 2 m no-reflection area where the railroad debris fill is missing (Fig. 13). The cave infills of the Gran Dolina and TR21 should be found undisturbed under the railroad fillings, as these are visible again on top of these caves.

The recent anthropic fillings are related to the artificial mound of sediments that existed in the railroad trench at the level of the Propiedad Valley, which facilitated the passage across the railroad and also marked the limit of two different villages (Ibeas de Juarros and Atapuerca) (Fig. 5B). This mound was dismantled in 1998 and the debris used to create a homogeneous flat surface all along the trench, which according to the GPR profiles and to historic photographs, raised the level of the surface up to 4 m in some areas (Figs. 5B and 12B).

5.3. Final remarks

A complete and thorough interpretation of the karstic and anthropic structures of the Thinchera area has only been possible because we considered the information of both the GPR profiles and the amplitude maps in horizontal grids. In this sense, we could not have obtained information about the host rock layers if we had not analysed the changes visible in the reflection profiles, and it would also have been difficult to define the distribution of the different cave and anthropic features without projecting the amplitude reflection slice maps over the karstic features map. Such comparison, although always necessary when interpreting the results of a GPR survey, has proven to be crucial in an environment such as a karstic system, where the geometry of dissolution features and their infilling units change dramatically in short distances. Moreover, this work provides a new approach for interpreting other karstic features located outside the railroad trench, in the unexplored areas of the Sierra de Atapuerca where there is no evidence for the underlying structure.

6. Conclusion

GPR surveys at the Trinchera caves in Atapuerca have helped identifying a variety of karst features of archaeological and geological interest. We were able to distinguish between these features depending on their origin as well as to determine the extent of the areas altered by recent anthropic activity.

With regard to the karstic features, we have identified: a) the air-filled passage of the Peluda Cave, based on the radar wave polarity changes, and two unknown void chimneys; b) the distribution and bedding attitude of the limestone host rock, including true dip; c) sediment-filled caves, including known and unknown conduits, most of which are filled by clay sediments that attenuated the radar waves. Caves that do not show such attenuation are interpreted as containing other types of sediments, like sands or fluvial gravels.

Identifying different types of cave-fill sediments with GPR furnishes invaluable information for the study of the Sierra de Atapuerca karstic system. In combination with the data provided by other methods, it could help determine the chronology of a cave infill by the type of sediments. It also constitutes practical information for excavation strategies, as it facilitates locating the more susceptible sites of containing archaeological remains for future studies. In this sense, further GPR surveys with different frequency antennas could gain more information on the stratigraphy.

Additionally, the study of the cave infills has exposed an intense vadose entrenchment incision for all the caves of the intermediate level of the Trinchera area and a strong relationship with the lower level of the karst, as all the caves studied in this work extent towards the west under the railroad surface (Fig. 15).

This work has shown that GPR analysis should be conducted even in areas that contain electrically conductive materials, which could attenuate radar waves. Here we found that the radar wave attenuating cave fill sediments could be easily identified, especially when bounded by the highly reflective limestone bedrock. In the Trinchera area this has been especially useful for "filling in the gaps" of the extant cave maps, as most of the unexplored and/or unknown parts of the caves remain invisible as they are filled with sediments. In this sense, GPR is an effective tool for obtaining rapid three-dimensional information on complex structures of this sort.

As for the recent anthropic alterations, we have distinguished between: a) the debris fills produced during the construction of the railroad trench, which can be seen in the first metre of all profiles except in further altered areas; b) the traces of two limestone quarries: one open-air cut and one underground mine, which extraction process was documented thanks to historic photographs and to the recognition, in the GPR profiles, of the ramp used to extract the blocks; c) recent infills, mostly visible in the areas where the quarries left irregular surfaces.

Given the significance of the remains found in the sites of Trinchera, it is important that the original cave infillings, where the geological and archaeological context remains intact, were distinguished from modern fillings of anthropic origin. Defining the limits of these anthropic structures constitutes another tool for planning future excavations in the area.

Finally, we hope that this thorough analysis of GPR data could be of use not only for the Sierra de Atapuerca sites, but also for encouraging other researchers to use this method in karst areas. Although interpreting GPR data can sometimes be complicated, previous information on the site can be enough for interpreting small scale details that may not be appreciated using other geophysical methods, as shown in this work. An iterative interpretation using both standard types of cave mapping and GPR can produce very accurate three-dimensional analysis not possible in any other way.

Data availability

Datasets related to this article can be found at: https://mega.nz/#F! 8A4yhYBb!ihOiSk8aNTqz8y16yy9nqA

Declaration of competing interest

The authors declare that they have no known competing financial interests or personal relationships that could have appeared to influence the work reported in this paper.

References

Anthony, D.M., 2004. Multilevel caves and lansdcape evolution. In: Culver, D., White, W. (Eds.), Encyclopedia of Caves. Academia Press, pp. 397–400.

Armenteros, I., Corrochano, A., Alonso-Gavilán, G., Carballeira, J., Rodríguez, J.M., 2002. Duero Basin (northern Spain). In: Gibbons, W., Moreno, T. (Eds.), Geology of Spain. Geol. Soc., London, pp. 309–315.

Arnold, L.J., Demuro, M., Parés, J.M., Pérez-González, A., Arsuaga, J.L., Bermúdez de Castro, J.M., Carbonell, E., 2015. Evaluating the suitability of extended-range luminescence dating techniques over early and Middle Pleistocene timescales: published datasets and case studies from Atapuerca. Spain. Quat. Int. 389, 167–190. https://doi.org/10.1016/j.quaint.2014.08.010.

Benito-Calvo, A., Pérez-González, A., 2007. Erosion surfaces and Neogene landscape evolution in the NE Duero Basin (north-central Spain). Geomorphology 88 (3–4), 226–241. https://doi.org/10.1016/j.geomorph.2006.11.005.

Benito-Calvo, A., Pérez-González, A., 2015. Geomorphology of the Sierra de Atapuerca and the Middle Arlanzón Valley (Burgos, Spain). Journal of Maps 11 (4), 535–544. https://doi.org/10.1080/17445647.2014.909339.

Benito-Calvo, A., Pérez-González, A., Parés, J.M., 2008. Quantitative reconstruction of Late Cenozoic landscapes: a case study in the Sierra de Atapuerca (Burgos, Spain). Earth Surf. Process. Landforms 33, 196–208. https://doi.org/10.1002/esp.1534.

Benito-Calvo, A., Ortega, A.I., Pérez-González, A., Campaña, I., Bermúdez de Castro, J.M., Carbonell, E., 2017. Palaeogeographical reconstruction of the Sierra de Atapuerca Pleistocene sites (Burgos, Spain). Quat. Int. 433 (PA), 379–392. https://doi.org/10.1016/j.quaint.2015.10.034.

Berger, G.W., Pérez-González, A., Carbonell, E., Arsuaga, J.L., Bermúdez de Castro, J.M., Ku, T.-L., 2008. Luminescence chronology of cave sediments at the Atapuerca paleoanthropological site, Spain. J. Hum. Evol. 55 (2), 300–311. https://doi.org/10.1016/j.jhevol.2008.02.012.

Bermejo, L., Ortega, A.I., Piro, S., Guérin, R., Conyers, L.B., Parés, J.M., Benito-Calvo, A., Campaña, I., Bermúdez de Castro, J.M., Carbonell, E., 2016. GPR data to constrain ERT interpretations in the archaeological karstic test site of Sierra de Atapuerca (Burgos, Spain). 6th Annual Meeting of the European Society for the study of Human Evolution (ESHE). Book of Abstracts, p. 50.

Bermejo, L., Ortega, A.I., Guérin, R., Benito-Calvo, A., Pérez-González, A., Parés, J.M., Aracil, E., Bermúdez de Castro, J.M., Carbonell, E., 2017. 2D and 3D ERT imaging for identifying karst morphologies in the archaeological sites of Gran Dolina and Galería Complex (Sierra de Atapuerca, Burgos, Spain). Quat. Int. 433 (PA), 393–401. https://doi.org/10.1016/j.quaint.2015.12.031.

Bermejo, L., Ortega, A.I., Conyers, L.B., Benito-Calvo, A., Parés, J.M., Bermúdez de Castro, J.M., Carbonell, E., 2018. Assessing the accuracy of 3D GPR results by comparing them to 3D laser scanner models: the case study of the archaeological site of Peluda Cave (Sierra de Atapuerca, Burgos, Spain). EGU General Assembly Conference Abstracts 20 , p. 1293. https://ui.adsabs.harvard.edu/abs/2018EGUGA..20.1293B.

Bermúdez de Castro, J.M., Arsuaga, J.L., Carbonell, E., Rosas, A., Martínez, I., Mosquera, M., 1997. A hominid from the Lower Pleistocene of Atapuerca, Spain: possible ancestor to Neandertals and modern human. Science 276 (5317), 1392–1395. https://doi.org/10.1126/science.276.5317.1392.

Campaña, I., 2018. Estratigrafía y sedimentología del yacimiento de Gran Dolina (Sierra de Atapuerca, Burgos). (Ph.D. Dissertation). Universidad de Burgos. CENIEH.

Campaña, I., Benito-Calvo, A., Pérez-González, A., Bermúdez de Castro, J.M., Carbonell, E., 2016. Assessing automated image analysis of sand grain shape to identify sedimentary facies, Gran Dolina archaeological site (Burgos, Spain). Sedimentary Geology 346, 72–83. https://doi.org/10.1016/j.sedgeo.2016.09.010.

Campaña, I., Benito-Calvo, A., Pérez-González, A., Ortega, A.I., Bermúdez de Castro, J.M., Carbonell, E., 2017. Pleistocene sedimentary facies of the Gran Dolina archaeo-paleoanthropological site (Sierra de Atapuerca, Burgos, Spain). Quat. Int. 433 (PA), 68–84. https://doi.org/10.1016/j.quaint.2015.04.023.

Carbonell, E., Rosas, A., Díez, J.C. (Eds.), 1999. Atapuerca: Ocupaciones Humanas y Palaeoecología del Yacimiento de Galería. Arqueología en Castilla y León, Memorias 7. Junta de Castilla y León, Valladolid.

Carbonell, E., Bermúdez de Castro, J.M., Parés, J.M., Pérez-González, A., Cuenca-Bescós, G., Ollé, A., Mosquera, M., Huguet, R., van der Made, J., Rosas, A., Sala, R., Vallverdú, J., García, N., Granger, D.E., Martinón-Torres, M., Rodríguez, X.P., Stock, G.M., Vergés, J.M., Allué, E., Burjachs, F., Cáceres, I., Canals, A., Benito-Calvo, A., Díez, C., Lozano, M., Mateos, A., Navazo, M., Rodríguez, J., Rosell, J., Arsuaga, J.L., 2008. The first hominin of Europe. Nature 425, 465–470. https://doi.org/10.1038/nature06815.

Chalikakis, K., Plagnes, V., Guérin, R., Valois, R., Bosch, F.P., 2011. Contribution of geophysical methods to karst-system exploration: an overview. Hydrogeol. J. 19, 1169–1180. https://doi.org/10.1007/s10040-011-0746-x.

Conyers, L.B., 2012. Interpreting Ground-penetrating Radar for Archaeology. Routledge, Taylor and Francis Group, New York.

Conyers, L.B., 2013. Ground-penetrating Radar for Archaeology. 3rd edn. Rowman and Littlefield, Lantham, MD, USA.

Deiana, R., Leucci, G., Martorana, R., 2018. New perspectives on geophysics for archaeology: a special issue. Surv. Geophys. 39, 1035–1038. https://doi.org/10.1007/s10712-018-9500-4.

Demuro, M., Arnold, L.J., Parés, J.M., Pérez-González, A., Ortega, A.I., Arsuaga, J.L., Bermúdez de Castro, J.M., Carbonell, E., 2014. New luminescence ages for the Galería Complex archaeological site: resolving chronological uncertainties on the acheulean record of the Sierra de Atapuerca, northern Spain. Plos One 9 (10), e110169. https://doi.org/10.1371/journal.pone.0110169.

Doolittle, J.A., Minzenmayer, F.E., Waltman, S.W., Benham, E.C., Tuttle, J.W., Peaslee, S.D., 2007. Ground-penetrating radar soil suitability map of the conterminous United States. Geoderma 141 (3–4), 416–421. https://doi.org/10.1016/j.geoderma.2007.05.015.

Eraso, A., Domínguez, M.C., Pérez-González, A., Martín, M.A., Ortega, A.I., 1998. Estimación de las paleovelocidades y sentidos de circulación del agua en el karst donde se emplaza el yacimiento arqueológico de la Sierra de Atapuerca (Burgos). Geogaceta. 23, pp. 39–42.

Falguères, C., Bahain, J.-J., Bischoff, J.L., Pérez-González, A., Ortega, A.I., Ollé, A., Quiles, A., Ghaleb, B., Moreno, D., Dolo, J.-M., Shao, Q., Vallverdú, J., Carbonell, E., Bermúdez de Castro, J.M., Arsuaga, J.L., 2013. Combined ESR/U-series chronology of Acheulian hominid-bearing layers at Trinchera Galería site, Atapuerca, Spain. J. Hum. Evol. 65 (2), 168–184. https://doi.org/10.1016/j.jhevol.2013.05.005.

Fernández-Jalvo, Y., 1995. Small mammal taphonomy at La Trinchera de Atapuerca (Burgos, Spain). A remarkable example of taphonomic criteria used for stratigraphic correlations and palaeoenvirnment interpretations. Palaeogeography, Palaeoclimatology, Palaeoecology 114, 167–195.

Ford, D.C., Williams, P., 1989. Karst Hydrogeology and Geomorphology. Unwin Hyman Ltd., London.

Gaffney, C., 2008. Detecting trends in the prediction of the buried past: a review of geophysical techniques in archaeology. Archaeometry 50 (2), 313–336. https://doi.org/10.1111/j.1475-4754.2008.00388.x.

Gil, E., Aguirre, E., Hoyos, M., 1987. Contexto estratigráfico. In: Aguirre, E., Carbonell, E., Bermudez de Castro, J.M. (Eds.), El hombre fósil de Ibeas y el Pleistoceno de la Sierra de Atapuerca. Junta de Castilla y León, Consejería de Cultura y Bienestar Social, Valladolid, pp. 45–47.

Hesse, A., 2002. Méthodes géophysiques de la prospection. In: Miskovsky, J.C. (Ed.), Géologie de la Préhistoire, 2nd edn. Association pour l'étude de l'environnement géologique de la Préhistoire, Paris, Géopré, pp. 393–406.

Huguet, R., Vallverdú, J., Rodríguez-Álvarez, X.P., Terradillos-Bernal, M., Bargalló, A., Lombera-Hermida, A., Menéndez, L., Modesto-Mata, M., Van der Made, J., Soto, M., Blain, H.-A., García, N., Cuenca-Bescós, G., Gómez-Merino, G., Pérez-Martínez, R., Expósito, I., Allué, E., Rofes, J., Burjachs, F., Canals, A., Bennàsar, M., Nuñez-Lahuerta, C., Bermúdez de Castro, J.M., Carbonell, E., 2017. Level TE9c of Sima del Elefante (Sierra de Atapuerca, Spain): a comprehensive approach. Quat. Int. 433 (PA), 278–295. https://doi.org/10.1016/j.quaint.2015.11.030.

Kaufmann, O., Deceuster, J., 2014. Detection and mapping of ghost-rock features in the Tournaisis area through geophysical methods: an overview. Geol. Belg. 17 (1), 17–26.

Martínez-Moreno, F.J., Galindo-Zaldívar, J., Pedrera, A., Teixido, T., Ruano, P., Peña, J.A., González-Castillo, L., Ruiz-Constán, A., López-Chicano, M., Martín-Rosales, W., 2014. Integrated geophysical methods for studying the karst system of Gruta de las Maravillas (Aracena, Southwest Spain). Journal of Applied Geophysics 107, 149–162. https://doi.org/10.1016/j.jappgeo.2014.05.021.

Moreno, D., Falguères, C., Pérez-González, A., Voinchet, P., Ghaleb, B., Despriée, J., Bahain, J.-J., Sala, R., Carbonell, E., Bermúdez de Castro, J.M., Arsuaga, J.L., 2015. New radiometric dates on the lowest stratigraphical section (TD1 to TD6) of Gran Dolina site (Atapuerca, Spain). Quaternary Geochronology 30 (PB), 535–540. https://doi.org/10.1016/j.quageo.2015.05.007.

Ollé, A., Mosquera, M., Rodríguez, X.P., Lombera-Hermida, A., García-Antón, M.D., García-Medrano, P., Peña, L., Menéndez, L., Navazo, M., Terradillos, M., Bargalló, A., Márquez, B., Sala, R., Carbonell, E., 2013. The Early Middle Pleistocene technological record from Sierra de Atapuerca (Burgos, Spain). Quat. Int. 295, 138–167. https://doi.org/10.1016/j.quaint.2011.11.009.

Ortega, A.I., 2009. La evolución geomorfológica del karst de la Sierra de Atapuerca (Burgos) y su relación con los yacimientos pleistocenos que contiene. (Ph.D. Dissertation). Universidad de Burgos.

Ortega, A.I., Benito-Calvo, A., Pérez-González, A., Porres, A., Martín, M.A., 2010. Applying electrical resistivity tomography to the identification of endokarst geometries in the Pleistocene sites of the Sierra de Atapuerca (Burgos, Spain). Archaeological Prospection 17, 233–245. https://doi.org/10.1002/arp.392.

Ortega, A.I., Benito-Calvo, A., Pérez-González, A., Martín-Merino, M.A., Pérez-Martínez, R., Parés, J.M., Aramburu, A., Arsuaga, J.L., Bermúdez de Castro, J.M., Carbonell, E., 2013. Evolution of multilevel caves in the Sierra de Atapuerca (Burgos, Spain) and its relation to human occupation. Geomorphology 196, 122–137. https://doi.org/10.1016/j.geomorph.2012.05.031.

Ortega, A.I., Benito-Calvo, A., Pérez-González, A., Carbonell, E., Bermúdez de Castro, J.M., Arsuaga, J.L., 2014. Atapuerca karst and its palaeoanthropological sites. In: Gutiérrez, F., Gutiérrez, M. (Eds.), Landscapes and Landforms of Spain. World Geomorphological Landscapes. Springer, Dordrecht, pp. 101–110 https://doi.org/10.1007/978-94-017-8628-7_8.

Ortega, A.I., Benito-Calvo, A., Martín, M.A., Pérez-González, A., Parés, J.M., Bermúdez de Castro, J.M., Arsuaga, J.L., Carbonell, E., 2018. Las cuevas de la Sierra de Atapuerca y el uso humano del paisaje kárstico durante el Pleistoceno (Burgos, España). Boletín Geológico y Minero 129 (1/2), 83–105. https://doi.org/10.21701/bolgeomin.129.1.004.

Parés, J.M., Pérez González, A., Rosas, A., Benito-Calvo, A., Bermúdez de Castro, J.M., Carbonell, E., Huguet, R., 2006. Matuyama-age lithic tools from the Sima del Elefante site, Atapuerca (northern Spain). J. Hum. Evol. 50 (2), 163–169. https://doi.org/10.1016/j.jhevol.2005.08.011.

Parés, J.M., Álvarez-Posada, C., Sier, M., Moreno, D., Duval, M., Woodhead, J., Ortega, A.I., Campaña, I., Rosell, J., Bermúdez de Castro, J.M., Carbonell, E., 2018. Chronology of

the cave interior sediments at Gran Dolina archaeological site, Atapuerca (Spain). Quat. Sci. Rev. 186, 1–16. https://doi.org/10.1016/j.quascirev.2018.02.004.

Pérez-González, A., Parés, J.M., Gallardo, J., Aleixandre, T., Ortega, A.I., Pinilla, A., 1999. Geología y estratigrafía del relleno de Galería de la Sierra de Atapuerca (Burgos). In: Carbonell, E., Rosas, A., Díez, J.C. (Eds.), Atapuerca: Ocupaciones humanas y paleoecología del yacimiento de Galería. Junta de Castilla y León, Consejería de Educación y Cultura, Valladolid, pp. 31–42.

Pérez-González, A., Parés, J.M., Carbonell, E., Aleixandre, T., Ortega, A.I., Benito-Calvo, A., Martín, M.A., 2001. Géologie de la Sierra de Atapuerca et stratigraphie des remplissages karstiques de Galería et Dolina (Burgos, Espagne). L'Anthropologie 105 (1), 27–43. https://doi.org/10.1016/S0003-5521(01)80004-2.

Pineda, A., Arce, J.M., 1997. Mapa Geológico de España, E 1:50.000, Hoja n°200 (Burgos), Serie Magna. IGME, Madrid.

Piscitelli, S., Rizzo, E., Cristallo, F., Lapenna, V., Crocco, L., Persico, R., Soldovieri, F., 2007. GPR and microwave tomography for detecting shallow cavities in the historical area of "Sassi of Matera (southern Italy)". Near Surface Geophysics 5 (4), 275–284. https://doi.org/10.3997/1873-0604.2007009.

Revil, A., Karaoulis, M., Johnson, T., Kemna, A., 2012. Review: some low-frequency electrical methods for subsurface characterization and monitoring in hydrogeology. Hydrogeol. J. 20 (4), 617–658. https://doi.org/10.1007/s10040-011-0819-x.

Rodríguez-Hidalgo, A., Saladié, P., Ollé, A., Arsuaga, J.L., Bermúdez de Castro, J.M., Carbonell, E., 2017. Human predatory behaviour and the social implications of comunal hunting based on evidence from the TD10.2 bison bone bed at Gran Dolina (Atapuerca, Spain). J Hum Evol 105, 89–122. https://doi.org/10.1016/j.jhevol.2017.01.007.

Rosas, A., Pérez-González, A., Carbonell, E., Van der Made, J., Sánchez-Marco, A., Laplana, C., Cuenca-Bescós, G., Parés, J.M., Huguet, R., 2001. Le gisement pléistocene de la Sima del Elefante (Sierra de Atapuerca, Espagne). L'Anthropologie 105 (2), 301–312. https://doi.org/10.1016/S0003-5521(01)80018-2.

Rosas, A., Huguet, R., Pérez González, A., Carbonell, E., Bermúdez de Castro, J.M., Vallverdú, J., Van der Made, J., Allué, E., García, N., Pérez-Martínez, R., Rodríguez, J., Sala, R., Saladié, P., Benito-Calvo, A., Martínez-Maza, C., Bastir, M., Sanchez, A., Parés, J.M., 2006. The Sima del Elefante cave site at Atapuerca (Spain). Estudios Geológicos 62 (1), 327–348. https://doi.org/10.3989/egeol.0662129.

Schrott, L., Sass, O., 2008. Application of field geophysics in geomorphology: advances and limitations exemplified by case studies. Geomorphology 93 (1), 55–73. https://doi.org/10.1016/j.geomorph.2006.12.024.

Valois, R., Bermejo, L., Guérin, R., Hinguant, S., Pigaud, R., Rodet, J., 2010. Karst morphologies identified with geophysics around Saulges caves (Mayenne, France). Archaeological Prospection 17 (3), 151–160. https://doi.org/10.1002/arp.385.

Weinstein-Evron, M., Beck, A., Ezersky, M., 2003. Geophysical investigations in the service of Mount Carmel (Israel). Journal of Archaeological Science 30 (10), 1331–1341. https://doi.org/10.1016/S0305-4403(03)00023-2.